forests

MDPI

Article

A Structural Assessment of Sycamore Maple Bark Disintegration by *Nectria cinnabarina*

Vladimír Račko [1], Ján Kováč [2], Oľga Mišíková [1], Ivan Mihál [3], Ivan Milenković [4,5] and Jaroslav Ďurkovič [2,*]

1 Department of Wood Science, Technical University in Zvolen, T.G. Masaryka 24, 96001 Zvolen, Slovakia; racko@tuzvo.sk (V.R.); misikova@tuzvo.sk (O.M.)
2 Department of Phytology, Technical University in Zvolen, T.G. Masaryka 24, 96001 Zvolen, Slovakia; kovacj@tuzvo.sk
3 Institute of Forest Ecology, Slovak Academy of Sciences, Štúrova 2, 96053 Zvolen, Slovakia; mihal@ife.sk
4 Faculty of Forestry, University of Belgrade, Kneza Višeslava 1, 11030 Belgrade, Serbia; ivan.milenkovic@sfb.bg.ac.rs
5 Phytophthora Research Centre, Faculty of Forestry and Wood Technology, Mendel University in Brno, 61300 Brno, Czech Republic
* Correspondence: jaroslav.durkovic@tuzvo.sk

Abstract: Previous phytopathological studies of the fungal pathogen *Nectria cinnabarina* have been focused on its distribution and host diversity but little is known about the spread of this pathogen and the defence responses of forest trees to an infection inside host tissues. Histopathological alterations of bark, periderm, phloem and woody tissues were investigated in sycamore maple (*Acer pseudoplatanus*) branches following their natural attack by the advanced anamorph and teleomorph developmental stages of the fungus. Light, fluorescence, confocal laser scanning and scanning electron microscopy techniques supplemented by X-ray micro-computed tomography imaging were used to distinguish between healthy and disintegrated plant tissues. The intercellular spread of fungal hyphae was found primarily in the phelloderm. Expanding hyphae aggregations produced ruptures in the phellem and the disintegration of both phellogen and phellodermal parenchyma cells in close proximity to the expanding fruiting bodies of the fungus. Thicker hyphae of the teleomorph fungal stage heavily disintegrated the phelloderm tissues and also induced enhanced sclerification of the nearby phloem tissues that limited the spread of the infection into the sieve tubes. Both the intercellular and intracellular spread of hyphae inside the peripheral parts of sclereid clusters led to the disintegration of the compound middle lamellae but the hyphae were only rarely able to pass through these structural phloem barriers. The massive fungal colonization of both lumens and disintegrated tangential cell walls of ray parenchyma cells resulted in severe cambial necroses. Although the hyphae penetrated into the outermost annual growth rings of the xylem, no cell wall disintegration of the parenchyma cells, vessels and fibres was revealed. Despite the local cambial necroses and severe phloem ray disintegration, the bark remained attached to the examined branches and no bark cankers were formed.

Keywords: *Acer pseudoplatanus*; *Tubercularia vulgaris*; fruit body; periderm; phloem; cambium

check for updates

Citation: Račko, V.; Kováč, J.; Mišíková, O.; Mihál, I.; Milenković, I.; Ďurkovič, J. A Structural Assessment of Sycamore Maple Bark Disintegration by *Nectria cinnabarina*. *Forests* **2022**, *13*, 452. https://doi.org/10.3390/f13030452

Academic Editor: Leena Hamberg

Received: 15 February 2022
Accepted: 3 March 2022
Published: 13 March 2022

Publisher's Note: MDPI stays neutral with regard to jurisdictional claims in published maps and institutional affiliations.

Copyright: © 2022 by the authors. Licensee MDPI, Basel, Switzerland. This article is an open access article distributed under the terms and conditions of the Creative Commons Attribution (CC BY) license (https://creativecommons.org/licenses/by/4.0/).

1. Introduction

The fungus *Nectria cinnabarina* (Tode) Fr. is the type species of the genus *Nectria* that belongs to the family Nectriaceae [1–3], order Hypocreales [4]. This fungus is a weak pathogen, attacking bark and outer sapwood of plants damaged by frost, water stress and mechanical wounds. In addition, the pathogen frequently occurs on dead stems and branches previously attacked by other pathogens [5]. Spores are dispersed from the fruiting bodies (FBs) that exude spores in rainy conditions or during irrigation [6]. The first visible symptom of *N. cinnabarina* on the attacked tree is the loss of the tree crown's density as a

result of both the breaks and dieback of thin branches. The infection spreads effectively during tree dormancy in winter, and less frequently during the growing season. The older mycelia lose their virulence; therefore, the fungus often survives in the saprotrophic phase under natural conditions. When attacked by the fungus, mature, coarse branches in the upper parts of the crowns fall down faster than younger and thinner ones [7].

Bionomy and life form characteristics of *N. cinnabarina* were described in detail by Hirooka et al. [1]. In the parasitic phase, *N. cinnabarina* is responsible for the canker formation in many hardwood trees and woody shrubs [8]. The parasitic growth of the fungus was first reported by Mayr [9] who considered this species to be parasitic on *Acer*, *Aesculus*, *Prunus*, *Robinia*, *Spiraea*, *Tilia*, and *Ulmus* [1]. Both saproparasitic and saprotrophic occurrence is very abundant on host taxa such as *Abies*, *Picea*, *Pinus*, *Fagus*, *Acer*, *Betula*, *Carpinus*, *Quercus* spp., *Fraxinus*, *Salix*, *Robinia*, *Tilia* spp., *Malus*, *Aesculus*, *Cerasus*, *Corylus*, *Sambucus*, *Sorbus* and *Juglans* [2]. In Slovakia, the occurrence of *N. cinnabarina* has been documented from at least 32 species of woody plants [10]. On the other hand, Jorgensen [11] demonstrated that *N. cinnabarina* was a facultative parasite and saprobe but could not differentiate the pathogenic races. Cankers appear as slightly sunken areas, generally associated with wounds [12,13]. However, they are not obvious until the emerging, orange-red perithecia develop in large quantities in the cankered area [6]. This species is characterized by red, globose, fleshy, warted perithecia that produce 0–3-septate ascospores and often become cupulate upon drying [1]. The anamorph stage has been referred to as *Tubercularia vulgaris* Tode [3,14] that has been commonly reported on woody substrates in many plant families [15]. *Tubercularia vulgaris* is also known as a canker pathogen on birch trees [16].

Sycamore maple (*Acer pseudoplatanus* L.) is one of the valuable noble hardwoods that is widespread through the European mixed forests. In the natural ecosystems, sycamore maple usually constitutes mixed stands, rarely pure stands. In addition, many cultivars are widely planted as popular ornamental or amenity trees [17]. There are numerous reports of various pathogenic organisms that are affecting sycamore maple trees such as *Verticillium* spp. [18], *Phytophthora* spp. [19,20] or *Cryptostroma corticale* (Ellis & Ever.) Greg. & Wall. [21]. In addition, sycamore maple trees are commonly reported as hosts of *N. cinnabarina* [2]. This fungus is one of the most frequent colonizers of sycamore maple, particularly if the trees are weakened or injured.

As the previous studies focused mainly on the distribution and host diversity of *N. cinnabarina* worldwide [1,11,22,23], little is known about the mechanisms of the infection and the spread of this pathogen inside the host phloem and xylem tissues. The aim of this anatomical study was to assess the differences in the extent of bark disintegration between the advanced teleomorph and anamorph developmental stages of *N. cinnabarina* following the attack of juvenile sycamore maple branches. The emphasis was given on the spread of the fungal infection inside the periderm, phloem and xylem tissues with respect to the induced structural defence responses of the host.

2. Materials and Methods

2.1. Plant and Fungal Materials

One branch containing the anamorph developmental stage of *N. cinnabarina* and one branch containing the teleomorph stage (both branches infected naturally, at least 15 years of age, 30 mm thick and 150 mm long), were sampled from the crown of a mature *A. pseudoplatanus* tree, at least 50 years of age (Figure 1). The age of branches was determined based on the number of annual growth rings. The attacked tree grows at Vrch Dobroč, Veporské vrchy Mts., Slovakia (48°31′42.9″ N, 19°34′16.1″ E, 820 m a.s.l.). Fungus determination was based on the morphological assessment of FBs according to the studies of Breitenbach and Kränzlin [24] and Rossman et al. [14]. Ten discs, 30 mm in diameter and 5 mm in length, were cut from each freshly sampled branch. Then, 10 samples (10 mm × 5 mm × 5 mm) including the FBs, bark, cambium and xylem, were extracted from the marginal parts of each disc. The samples were divided into three subsets for

various types of microscopy. For histopathological observations, we used the sections of host tissues that were sampled directly beneath the FBs of *N. cinnabarina*.

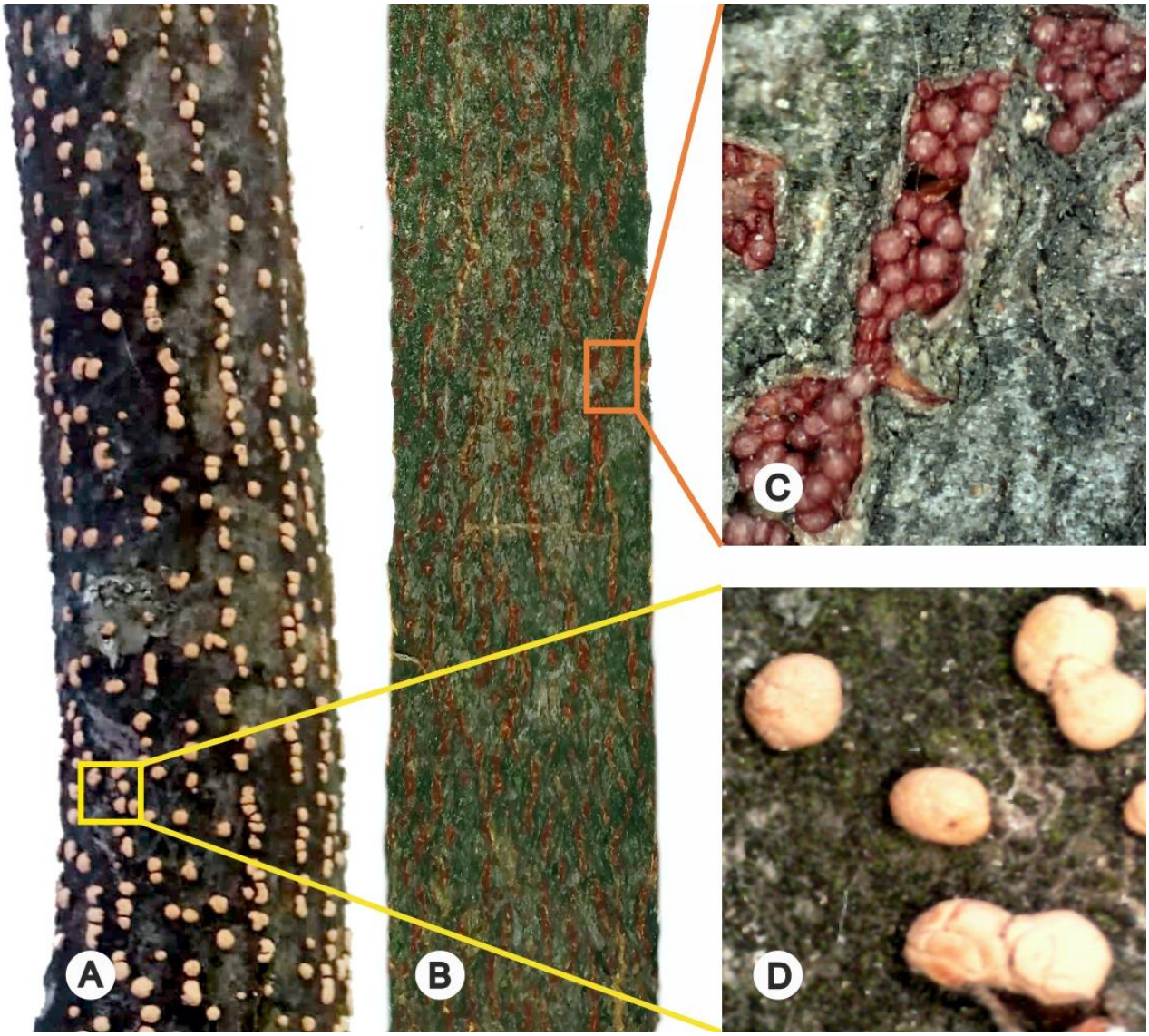


Figure 1. Sycamore maple branch attacked by *Nectria cinnabarina* fruiting bodies in the anamorph (**A**) and teleomorph (**B**) developmental stages, respectively. The closeup view of fruiting bodies in the anamorph (**D**) and teleomorph (**C**) stages, respectively.

2.2. Light Microscopy

On the bark surface, the width, length and area of cracks in phellem as well as the number of FBs were measured on fresh specimens using the light microscope Dino-Lite Edge 3.0 (AnMo Electronics Corp., New Taipei City, Taiwan). Afterwards, the same samples were embedded in polyethylene glycol PEG 1500 following the procedure of Račko et al. [25], and trimmed with a sledge microtome (Reichert, Vienna, Austria) until the cross-sectional cutting plane was positioned in the centre of FB. Both height and width of FBs and the maximal width of phellem separation by stroma were determined using the light microscope Dino-Lite Edge 3.0 (Figure 2).

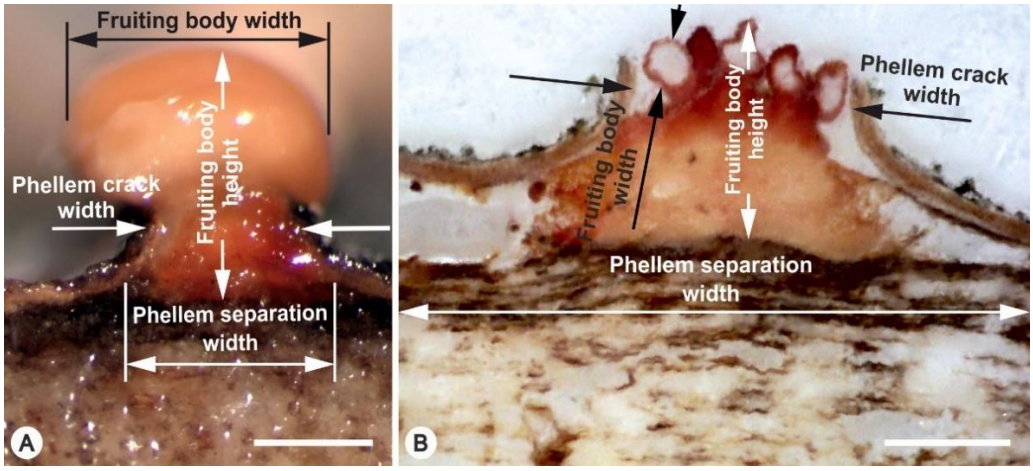


Figure 2. The scheme of fruiting body size measurements in the anamorph (**A**) and teleomorph (**B**) stages, respectively. Cross-sections, scale bars = 500 µm.

Twenty-micrometer-thick cross-sections from the central parts of FBs were prepared for the transmission light microscopy according to the protocol of Račko et al. [25]. The cross-sections were stained with the multichromatic dye Toluidine blue O (Sigma-Aldrich, St. Louis, MO, USA) according to the protocol of O'Brien et al. [26] to distinguish lignified tissues, non-lignified tissues and polyphenolic compounds. The cross-sections were observed using an Axio Lab.A1 microscope (Carl Zeiss Microscopy, Jena, Germany) equipped with a Canon EOS 600D camera (Canon Inc., Tokyo, Japan).

2.3. Fluorescence and Confocal Laser Scanning Microscopy

For a better discrimination of various bark components and fungal hyphae, both fluorescence and confocal laser scanning microscopy techniques were used. The second subset of samples (3 mm × 3 mm × 5 mm) was embedded in Technovit 7100 embedding medium (Heraeus Kulzer GmbH, Wehrheim, Germany) according to the protocol of Yeung and Chan [27]. Cross-sections, approximately five-micrometer-thick, were cut using a rotary microtome Leica RM2255 (Leica Biosystems, Nussloch, Germany) and glass knives, submerged in a drop of 50% glycerol, and observed using a fluorescence microscope Leica DM4000 B (Leica Microsystems, Wetzlar, Germany) equipped with a digital color camera Leica DFC490 and a cube filter H3 (BP 420–490 nm/LP 515 nm). For confocal laser scanning microscopy, an instrument Olympus FluoView FV1200 (Olympus, Tokyo, Japan) was used being equipped with 405, 473 and 635 nm exciting lasers. The emissions were detected in the ranges of 410–460 nm, 480–580 nm and 640–700 nm, respectively, for individual lasers.

2.4. Scanning Electron Microscopy

The third subset of samples was air-dried, mounted on specimen stubs using a carbon tape, sputter-coated with gold (layer thickness of 120 nm) in the Sputter Coater K650X (Quorum Technologies, Ashford, UK) under argon atmosphere, and examined by high-vacuum scanning electron microscopy using a JEOL JSM-6390LV instrument (JEOL, Tokyo, Japan) operating at 20 kV.

2.5. X-ray Micro-Computed Tomography

X-ray micro-computed tomography imaging of bark and woody tissues was performed with a Phoenix V | Tome | X L 240 device (GE Sensing & Inspection Technologies, Wunstorf, Germany) as described in detail by Karadžić et al. [28]. Three-dimensional data sets were evaluated using VGSTUDIO MAX 2.2 software for industrial computed tomography data (Volume Graphics, Heidelberg, Germany).

2.6. Statistical Analysis

Morphological traits of FBs and phellem cracks were analyzed using Student's *t*-test. The morphological data of fungal hyphae growing inside various cell types were analyzed using a one-way analysis of variance and Duncan's multiple range test to determine pairwise comparisons of means.

3. Results

3.1. Formation of FBs

Numerous FBs occurred on the bark surface of both branch specimens indicating the advanced anamorph (Figure 3A) and teleomorph (Figure 3B,C) stages of fungus development. The primary infection penetrated through the cracks in the periderm into drier but still living branches. This resulted in the growth of sporodochia inside the lumens of dying marginal phellodermal parenchyma cells. The intracellular growth of fungal hyphae caused a death of phellodermal parenchyma cells and disturbed their cell wall integrity. The growing intercellular stromata began to accumulate preferentially under the phellem bark layer. The stromata expansion pushed away the phellem layers which simultaneously resulted in the gradual tangential separation of the phellem from the phelloderm (Figure 3D). This expansion also led to a gradual disintegration of the phellogen layer. In the later stage, the pressure-stressed phellem layers cracked and juvenile FBs began to form inside the cavities (Figure 3E). Maturing FBs emerged through the cracks above the stem surface and their stromata bodies tightly filled the cavities beneath the phellem (Figure 3F). The anamorph stage formed a smaller stromata size than the teleomorph one. The separation of phellem and the dimensions of cracks in the phellem were also lesser in the anamorph stage (Table 1).

Table 1. Morphological traits of fruiting bodies (FBs) and phellem cracks.

Trait	Anamorph	Teleomorph	*p*-Value
FB density (min and max number per cluster)	1–3	9–23	
FB height (µm)	824 ± 110	606 ± 134	<0.0001 ***
FB width (µm)	854 ± 215	166 ± 43	<0.0001 ***
Phellem separation width (µm)	690 ± 179	1012 ± 258	<0.0001 ***
Phellem crack width (µm)	418 ± 153	688 ± 263	<0.0001 ***
Phellem crack length (µm)	560 ± 266	1263 ± 1307	0.0029 **
Phellem crack area (mm^2)	0.218 ± 0.134	0.455 ± 0.488	0.0086 **

Data represent means ± SD. *** indicates statistically significant difference at the level of $p < 0.001$ and ** at the level of $0.001 \leq p < 0.01$, respectively.

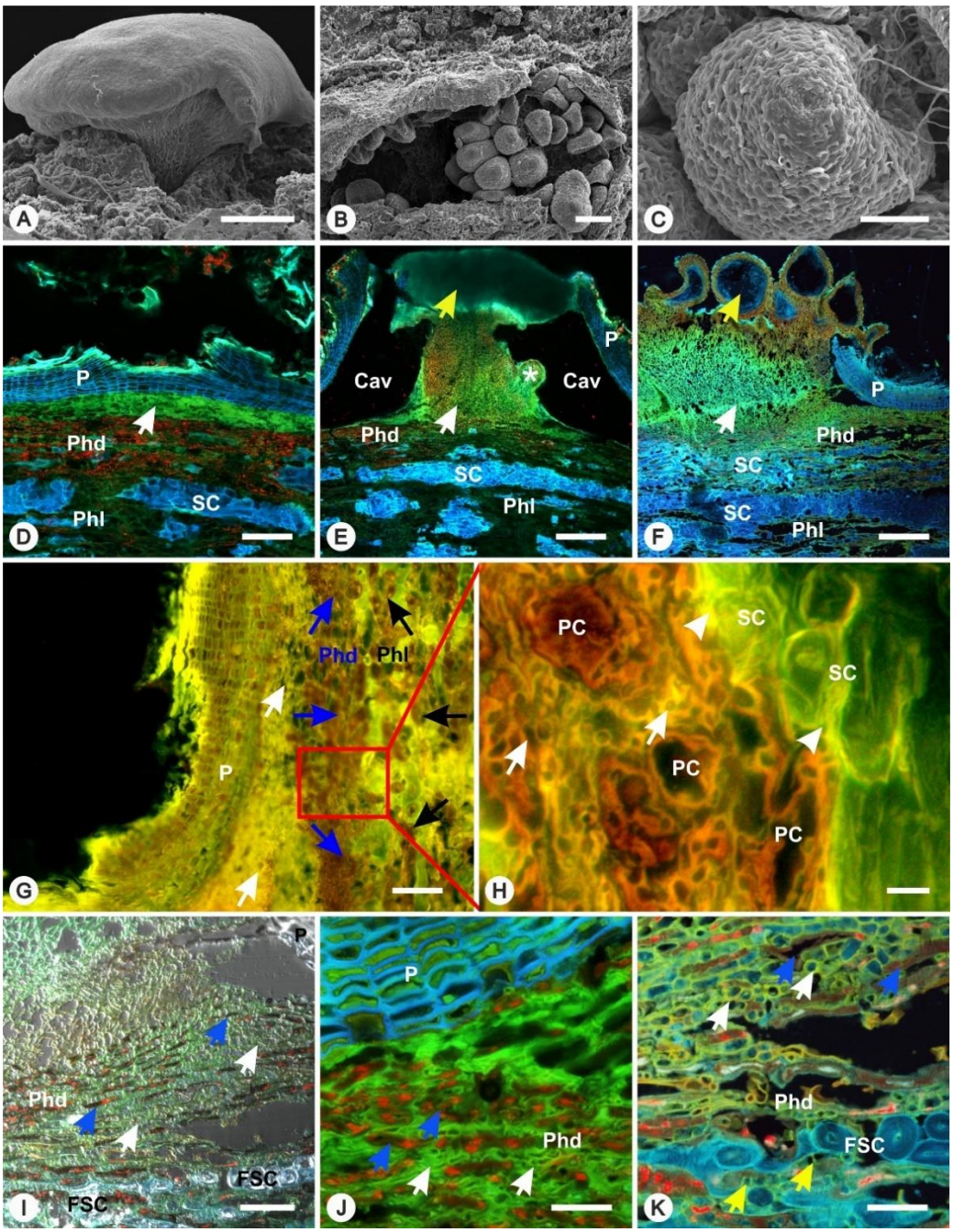


Figure 3. Histopathological assessments of the periderm layer disintegration using scanning electron (**A**–**C**), confocal laser scanning (**D**–**F**,**I**–**K**) and fluorescence (**G**,**H**) microscopies. (**A**) Fruiting bodies in the anamorph developmental stage. (**B**) Fruiting bodies in the teleomorph developmental stage. (**C**) A detailed view of the perithecium surface. (**D**) The early stage of the stroma (white arrows) that was formed between phelloderm and phellem layers. Cross-section. (**E**) Maturation of the anamorph fruiting bodies (conidioma) (yellow arrow) and the formation of new juvenile fruiting bodies (asterisk) on the stroma (white arrow). Cross-section. (**F**) Mature teleomorph perithecia (yellow arrow) outgrowing from the stroma (white arrow) in the crack of the phellem layer. Cross-section. (**G**) Juvenile stroma hyphae (white arrows), localized in between phellem and phelloderm layers, induced a deposition of brown colored polyphenolic compounds inside the living parenchyma cells of phelloderm (blue arrows) and phloem (black arrows). Radial section. (**H**) Closeup view of the previous image showing the intercellular hyphae (white arrows) that separated parenchyma cells and sclereid clusters in the phelloderm. White arrowheads point to the sites of the sclereid cluster

cell wall disintegration that was caused by the intercellular hyphae. Radial section. (**I**–**K**) Phelloderm disintegration by mature stromata hyphae (white arrows) in anamorph (**J**) and teleomorph (**I**,**K**) developmental stages. The expanding hyphae (white arrows) from both fungal developmental stages compressed and separated the individual parenchyma cells of phelloderm (blue arrows) that were filled with chlorophyll deposits (red color dots). Severe disintegration of fibre-sclereid clusters (yellow arrows) occurred especially in the teleomorph developmental stage (**K**). Cross-sections. Scale bars: (**A**,**B**,**D**–**F**) = 200 µm, (**I**) = 100 µm, (**C**,**G**) = 50 µm, (**J**,**K**) = 20 µm, (**H**) = 5 µm. Cav, cavity; FSC, fibre-sclereid cluster; P, phellem; PC, parenchyma cells; Phd, phelloderm; Phl, phloem; SC, sclereid cluster.

3.2. Spread of Infection Inside the Periderm

Thin fungal hyphae simultaneously penetrated deeper into the phelloderm through the pits of parenchyma cells and caused their death. This disturbation triggered massive defence responses in the surrounding living parenchyma cells including a deposition of brown colored polyphenolic compounds inside these cells (Figure 3G). Later, thin hyphae penetrated into the cell walls and intercellular spaces of the surrounding parenchyma cells where they became coarse. After that, parenchyma cells were separated by the expanding hyphae and their shape was deformated (Figure 3H).

3.3. Disintegration of the Periderm Layer

In the advanced stages of FB maturation, the growing hyphae mechanically disintegrated all phelloderm layers. The growing and expanding fungal mycelia inside the stromata induced the separation of deformed and mechanically disintegrated parenchyma cells (Figure 3I–K). The intercellular hyphae were more than two times thinner in the anamorph (Figure 3J) than in the teleomorph (Figure 3K) stage (Table 2). Massive disturbances in the phelloderm layers in close proximity to developing FBs were caused mainly by thick hyphae from the teleomorph stage.

Table 2. The width of fungal hyphae (in µm) inside periderm, phloem and xylem tissues.

Trait	Anamorph	Teleomorph	*p*-Value
Phelloderm parenchyma cells	1.5 ± 0.5^{a}	4.1 ± 0.2^{a}	<0.0001 ***
Phloem parenchyma cells	1.1 ± 0.5^{b}	2.0 ± 0.9^{b}	<0.0001 ***
Xylem parenchyma cells	1.6 ± 0.3^{a}	1.6 ± 0.4^{c}	0.9976 NS
Xylem vessels	0.6 ± 0.5^{c}	0.6 ± 0.5^{e}	0.8725 NS
Xylem fibres	1.3 ± 0.4^{b}	1.3 ± 0.4^{d}	0.7586 NS

Data represent means ± SD. Mean values followed by the same letters, a–e across examined cell types within the same column, are not significantly different at $p < 0.05$ (Duncan's multiple range test). Asterisks denote a significant difference within the same row between the anamorph and teleomorph developmental stage (Student's *t*-test). *** indicates statistically significant difference at the level of $p < 0.001$ and NS means non-significant difference, respectively.

3.4. Spread of Infection Inside Phloem Tissues

In the phelloderm tissues, we observed a high degree of fungal hyphae expansion and parenchyma cell disintegration. However, the fungus pathogenicity gradually weakened in the phloem tissues (Figure 4A), and no differences were found in the spread of the infection between both fungus developmental stages. The centripetal spread of the hyphae into the inner phloem tissues was limited by structural barriers comprised of frequently occurring sclereid clusters in the outer phloem. Enhanced sclerification was observed mainly at the teleomorph developmental stage of the fungus (Figure 3E,F). Parenchyma cells, located either between the sclereid clusters or the fibre-sclereids, were often sclerified in response to the spread of the infection. Tangential and radial expansions of smaller sclereid clusters in the phloem frequently resulted in merging to large sclereid ones (Figure 4B). Phenolic compounds were deposited into the lumens of parenchyma cells that were transforming to sclereids (Figure 4C). Deposits often penetrated through the pits into the adjacent tissues (Figure 4D). Degradations of thick cell walls were found in some sclereids and

fibre-sclereids (Figure 4E). The intercellular spread of the hyphae led to the disintegration of the compound middle lamellae in these sclereid cells (Figure 4E).

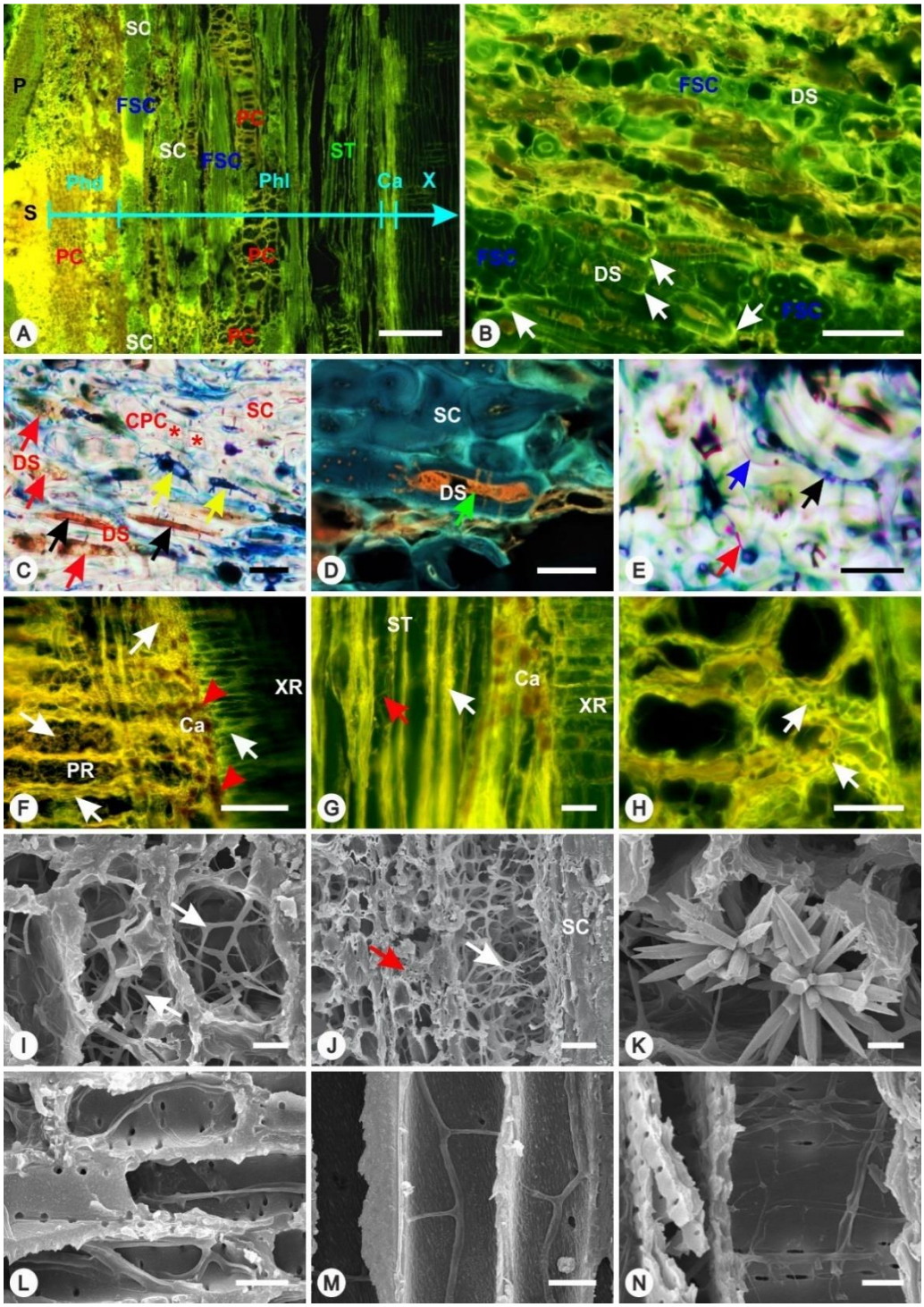


Figure 4. Histopathological assessments of the phloem and xylem tissue disintegration using fluorescence (**A**,**B**,**F**–**H**), light (**C**,**E**), confocal laser scanning (**D**) and scanning electron (**I**–**N**) microscopies. (**A**) The spread of the fungal infection through the parenchyma cells and the sclereid clusters of both phelloderm and phloem layers towards the cambium and xylem tissues. Yellow color denotes the hyphae aggregates in phelloderm and the disintegration of green colored lignocellulosic cell walls. Brown coloration indicates the presence of polyphenolic compounds in the parenchyma cell walls of both phelloderm and phloem. Radial section. (**B**) Developing sclereids, located between two mature

fibre-sclereid clusters, restricted the spread of the infection (yellow colored areas) into the inner phloem tissues. However, some hyphae penetrated also into the middle lamellae of developing sclereids (white arrows). Cross-section. (**C**) Different types of polyphenolic compounds (red, black and yellow arrows) or inorganic crystals (asterisks) found inside the lumens of developing sclereids and mature sclereid clusters or crystalliferous parenchyma cells. Cross-section. (**D**) Polyphenolic compounds (green arrow) inside the developing sclereid that protruded through the pits into adjacent cell walls. Cross-section. (**E**) The spread of the hyphae through the pits (red arrow) and degradations of both compound middle lamella (black arrow) and secondary cell wall (blue arrow). Cross-section. (**F**) The massive spread of the hyphae (arrow) through the parenchyma cells of phloem rays, cambial cells and parenchyma cells of xylem rays. Red arrowheads point to polyphenolic compounds inside the lumens of cambial cells. Radial section. (**G**) The spread of the hyphae (red arrow) inside the sieve tubes and disintegration of sieve cell walls (white arrow). The hyphae are visible also inside the cambium and parenchyma cells of the xylem ray. Radial section. (**H**) Disintegration of cell walls in dilatation parenchyma cells (white arrows). Radial section. (**I**) The hyphae aggregates inside the lumens of dilatation parenchyma cells (white arrows). Radial section. (**J**) Local aggregation of the hyphae inside the cavity in close proximity to a mature sclereid cluster. Red arrow shows the cell wall disintegration of adjacent parenchyma cells. Radial section. (**K**) The occasional formation of calcium oxalate crystals inside the lumens of inner phloem parenchyma cells. Radial section. (**L**) The spread of the hyphae inside the lumens of xylem ray parenchyma cells. Radial section. (**M**) Lumens of libriform fibres invaded by the hyphae. Radial section. (**N**) Hyphae growing inside an earlywood vessel. Radial section. Scale bars: (**A**) = 200 µm, (**B**,**F**) = 50 µm, (**C**–**E**,**G**,**H**,**J**) = 20 µm, (**I**,**L**–**N**) = 10 µm, (**K**) = 5 µm. Ca, cambium; CPC, crystalliferous parenchyma cells; DS, developing sclereids; FSC, fibre-sclereid clusters; P, phellem; PC, parenchyma cells; Phd, phelloderm; Phl, phloem; PR, phloem ray; S, stroma; SC, sclereid cluster; ST, sieve tube; X, xylem; XR, xylem ray.

Massive centripetal spread of the hyphae proceeded mainly through the phloem rays and axial parenchyma cell lumens, whereas inside the sieve tubes the hyphae density was low. The hyphae simultaneously attacked the tangential walls of ray parenchyma cells and caused their heavy disintegration. Afterwards, the infection spread along the radial and transverse cell walls towards the cambial zone. Around the sites of phloem ray cambium junctions, cambial cells necrotized and the hyphae penetrated into the xylem parenchyma rays (Figure 4F). Inside the phloem rays, the hyphae density decreased with the increasing longitudinal distance between the rays and the centre of the infection. No fungal attack of the cambium was found from the hyphae spreading through the farther phloem rays. However, both intercellular and intracellular spread of thin hyphae was observed inside the sieve tubes near the cambial zone, which caused severe local cambial necroses (Figure 4G).

Both axial and dilatation parenchyma cells were preferentially attacked near the sites of FB development. Again, the hyphae density decreased with the increasing longitudinal, radial and tangential distances from the centre of the infection. The hyphae strongly disintegrated the cell walls of dead parenchyma cells (Figure 4H) and their spread was observed again inside the lumens of parenchyma cells (Figure 4I). Local disintegration of cell walls in adjacent parenchyma cells supported a further accumulation of the hyphae inside the newly formed cavities in close proximity to sclereid clusters. These sclereid clusters limited the massive fungal colonization of inner phloem tissues (Figure 4J). Lumens of parenchyma cells were frequently filled with inorganic crystals. The elemental composition analysis revealed that the crystals were composed mostly of calcium oxalate (Figure 4K, Video S1).

3.5. Spread of Infection Inside Xylem Tissues

Xylem tissues were not heavily colonized by N. cinnabarina hyphae that were found only in the first two outermost annual growth rings (Figure 4F). The lumens of ray parenchyma cells were invaded mainly by thick hyphae (Figure 4L), whereas thin hyphae penetrated usually into the vessels and libriform fibres (Figure 4M,N and Table 2). The

overall spatial imaging of sycamore maple tissues infected with N. cinnabarina, including the anamorphic tuberculocidal FBs on the bark surface, is shown in Video S1.

4. Discussion

Although *N. cinnabarina* is considered to be a weaker saproparasitic pathogen, occurring predominantly on dying branches of stressed trees [5,11], our observations revealed that the fungus was capable to penetrate, colonize and significantly disintegrate the tissues of periderm, phloem and cambial zone in the advanced fungus developmental stages. Previous studies did not provide direct evidence whether or not *N. cinnabarina* is capable to disintegrate lignocellulosic cell wall structures of the bark [7,9,29]. The capability of lignocellulosic cell wall destruction has been confirmed for another taxon, *Neonectria ditissima* colonizing the apple host tree, where a clear collapse of the cortex and phloem cells was observed at day 29 post-inoculation [30]. Xiwang et al. [31] reported that the prominent intercellular spread of *Valsa mali* hyphae in the middle lamellae of apple phloem cells appeared between days 5 and 10 post-infection along with a significant decrease in the pectin content. Our study showed that sycamore maple cell walls were strongly disintegrated by *N. cinnabarina* hyphae. We observed heavy cell wall disintegration in the parenchyma cells of the phelloderm and phloem rays, whereas a weaker attack was recorded inside the sclereids and phloem fibres. Phloem rays served primarily as channels for the centripetal spread of the infection towards the cambial zone as it was also reported by Blanchette and Biggs [32].

In the early stages of the fungus development, the hyphae probably bypassed defence phellogen barriers when they penetrated through the pits of unplugged fibre lumens and their spread continued deeper into the phloem tissues as shown previously for apple trees infected with *Neonectria galligena* [33] and for poplars infected with *Cytospora chrysosperma* [34]. Additional inoculation trials with *N. cinnabarina* on various hosts are required to confirm these assumptions. However, in the advanced fungus developmental stages, enhanced sclerification that was induced by the infection significantly limited the spread of *N. cinnabarina* hyphae into the inner phloem tissues. Furthermore, the disintegration of sclereid secondary cell walls was rarely seen. The enlarged formation of sclereid clusters was also reported in the phloem tissues of *Fraxinus mandshurica* var. *japonica* trees infected with *Neonectria galligena* [35].

A pioneer phytopathological study, that was focused on the influence of *N. cinnabarina* on many host species [9], reported the highest susceptibility of Norway maple towards the fungus. The disease spread very effectively through the exposed xylem tissues, whereas the cortex and phloem tissues remained healthy for about 8 weeks. The hyphae penetrated through the xylem wounds into the lumens of vessels, fibres and ray parenchyma cells and were able to consume their content (starch, sugars and phenolic compounds). Later, the hyphae also infected drier bark tissues and thus, a disease progression continued [9]. On the other hand, Line [29] found that, in the early stages, *N. cinnabarina* hyphae feeding on red currant, lime and horse chestnut hosts were not able to severely attack the living parenchyma cells of both phloem and xylem rays. The spread of the infection was slow, but later the lumens of dying parenchyma cells were filled with the hyphae. Zalasky [36] reported that *Neonectria galligena* hyphae penetrated through the petiole bases and leaf traces into the periderm of aspen and willow hosts, but the resulting lesions were small and usually latent.

Compared to other *Nectria* and *Neonectria* pathogens, the main difference in the *N. cinnabarina* strategy of spread is a pattern of phloem tissue disintegration. While *Neonectria ditissima* in its advanced stages of development was capable of heavily destructing all cells of the host phloem tissues [30], our study demonstrated that *N. cinnabarina* disintegrated only tangential cell walls of ray parenchyma cells in the phloem. Cell walls of the sieve tubes remained compact. Despite the local cambial necroses and severe phloem ray disintegration, the bark remained attached to the examined branches and no bark cankers were formed.

Supplementary Materials: The following supporting information can be downloaded at: https://www.mdpi.com/article/10.3390/f13030452/s1, Video S1: X-ray micro-computed tomography radial imaging of sycamore maple bark and xylem tissues infected with *Nectria cinnabarina* in the anamorph developmental stage.

Author Contributions: V.R., O.M. and I.M. (Ivan Mihál) conceived the study and designed the experiment; I.M. (Ivan Mihál) identified and sampled biological materials; O.M. carried out light microscopy observations; V.R. and J.K. carried out fluorescence and confocal laser scanning microscopy observations; J.Ď. carried out scanning electron microscopy and X-ray micro-computed tomography imaging; V.R. analysed the data; V.R., J.Ď. and I.M. (Ivan Milenković) prepared the first draft. All authors have read and agreed to the published version of the manuscript.

Funding: This publication is the result of the projects implementations: FORRES (ITMS: 313011T678) and FOMON (ITMS: 313011V465) both of which were supported by the Operational Programme Integrated Infrastructure (OPII) funded by the European Regional Development Fund, and VEGA (1/0450/19 and 2/0045/22).

Data Availability Statement: Data are available on request from the corresponding author.

Conflicts of Interest: The authors declare no conflict of interest.

References

1. Hirooka, Y.; Rossman, A.Y.; Chaverri, P. A morphological and phylogenetic revision of the *Nectria cinnabarina* species complex. *Stud. Mycol.* **2011**, *68*, 35–56. [CrossRef]
2. Mihál, I. Occurrence of fungi of the genus *Nectria* s.l. (*Ascomycota*, *Hypocreales*, *Bionectriaceae*, *Nectriaceae*) in Slovakia. *Folia Oecol.* **2011**, *38*, 80–88.
3. Rossman, A.Y.; Seifert, K.A.; Samuels, G.J.; Minnis, A.M.; Schroers, H.J.; Lombard, L.; Crous, P.W.; Põldmaa, K.; Cannon, P.F.; Summerbell, R.C.; et al. Genera in *Bionectriaceae*, *Hypocreaceae*, and *Nectriaceae* (*Hypocreales*) proposed for acceptance or rejection. *IMA Fungus* **2013**, *4*, 41–51. [CrossRef]
4. Kirk, P.M.; Cannon, P.F.; Minter, D.W.; Stalpers, J.A. *Ainsworth & Bisby's Dictionary of Fungi*, 10th ed.; CAB International: Wallingford, UK, 2008; 771p.
5. Mitchell, C.P.; Ford-Robertson, J.B.; Hinckley, T.; Sennerby-Forsse, L. *Ecophysiology of Short Rotation Forest Crops*; Kluwer Academic Publishers: Dordrecht, the Netherlands, 1993; 308p.
6. Jones, R.K.; Benson, D.M. *Diseases of Woody Ornamentals and Trees in Nurseries*; American Phytopathological Society: St. Paul, MN, USA, 2001; 482p.
7. Uri, J. The parasitism of *Nectria cinnabarina* (Tode) Fr. *Tijdschr. Planteziekt.* **1948**, *54*, 29–73.
8. Sinclair, W.A.; Lyon, H.H. *Diseases of Trees and Shrubs*, 2nd ed.; Cornell University Press: Ithaca, NY, USA, 2005; 660p.
9. Mayr, H. *Über den Parasitismus von Nectria cinnabarina*; Springer: Berlin, Germany, 1882.
10. Račko, V.; Mihál, I.; Mišíková, O. Beech bark disease in Slovakia related to fungi of the genus *Nectria* s.l. and the anatomy of necrotised bark and wood: A brief review. *Folia Oecol.* **2020**, *47*, 16–22. [CrossRef]
11. Jorgensen, H.A. Studies on *Nectria cinnabarina*–hosts and variations. *Årsskr. K. Vet. Landbohøjsk.* **1952**, *35*, 57–120.
12. Bedker, P.J.; Blanchette, R.A. Development of cankers caused by *Nectria cinnabarina* on honey locusts after root pruning. *Plant Dis.* **1983**, *67*, 1010–1013. [CrossRef]
13. Bedker, P.J.; Blanchette, R.A.; French, D.W. *Nectria cinnabarina*: The cause of a canker disease of honey locust in Minnesota. *Plant Dis.* **1982**, *66*, 1067–1070. [CrossRef]
14. Rossman, A.Y.; Samuels, G.J.; Rogerson, C.T.; Lowen, R. Genera of *Bionectriaceae*, *Hypocreaceae* and *Nectriaceae* (*Hypocreales*, *Ascomycetes*). *Stud. Mycol.* **1999**, *42*, 1–248.
15. Seifert, K.A. *A Monograph of Stilbella and Some Allied Hyphomycetes*; Centraalbureau voor Schimmelcultures: Baarn, the Netherlands, 1985; 235p.
16. Grigaliūnaitė, B.; Burokienė, D.; Matelis, A.; Stackevičienė, E. Cancer diseases on birch (*Betula* L.) in Vilnius city green plantations. *Acta. Biol. Univ. Daugavp.* **2010**, *2*, 133–136.
17. Van Gelderen, D.M.; De Jong, P.C.; Oterdoom, H.J. *Maples of the World*; Timber Press: Portland, OR, USA, 1994; 478p.
18. Hiemstra, J.A.; Harris, D.C. *A Compendium of Verticillium Wilt in Tree Species*; Ponsen & Looijen: Wageningen, the Netherlands, 1998; 80p.
19. Milenković, I.; Nowakowska, J.A.; Oszako, T.; Mladenović, K.; Lučić, A.; Rakonjac, L.; Karadžić, D. Morphological and molecular identification of *Phytophthora* species from maple trees in Serbia. *Genetika* **2014**, *42*, 353–368. [CrossRef]
20. Tkaczyk, M.; Sikora, K.; Kunca, A. First report on the occurrence of *Phytophthora obscura* on *Acer pseudoplatanus* in Slovakia. *For. Pathol.* **2021**, *51*, e12686. [CrossRef]
21. Kelnarová, I.; Černý, K.; Zahradník, D.; Koukol, O. Widespread latent infection of *Cryptostroma corticale* in asymptomatic *Acer pseudoplatanus* as a risk for urban plantations. *For. Pathol.* **2017**, *47*, e12344. [CrossRef]

22. Yang, D.-Q. Isolation of wood-inhabiting fungi from Canadian hardwood logs. *Can. J. Microbiol.* **2005**, *51*, 1–6. [CrossRef]
23. Hirooka, Y.; Rossman, A.Y.; Samuels, G.J.; Lechat, C.; Chaverri, P. A monograph of *Allantonectria*, *Nectria*, and *Pleonectria* (*Nectriaceae*, *Hypocreales*, *Ascomycota*) and their pycnidial, sporodochial, and synnematous anamorphs. *Stud. Mycol.* **2012**, *71*, 1–210. [CrossRef]
24. Breitenbach, J.; Kränzlin, F. *Fungi of Switzerland. Vol. 1. Ascomycetes*; Verlag Mykologia: Lucerne, Switzerland, 1986; 412p.
25. Račko, V.; Mišíková, O.; Štefková, J.; Čunderlík, I. A fast method to prepare microslides of wood in advanced stages of decay. *IAWA J.* **2018**, *39*, 234–243. [CrossRef]
26. O'Brien, T.P.; Feder, N.; McCully, M.E. Polychromatic staining of plant cell walls by toluidine blue O. *Protoplasma* **1964**, *59*, 368–373. [CrossRef]
27. Yeung, E.C.; Chan, C.K.W. The Glycol Methacrylate Embedding Resins—Technovit 7100 and 8100. In *Plant Microtechniques and Protocols*; Yeung, E., Stasolla, C., Sumner, M., Huang, B., Eds.; Springer International Publishing: Cham, Switzerland, 2015; pp. 67–82.
28. Karadžić, D.; Stanivuković, Z.; Milanović, S.; Sikora, K.; Radulović, Z.; Račko, V.; Kardošová, M.; Ďurkovič, J.; Milenković, I. Development of *Neonectria punicea* pathogenic symptoms in juvenile *Fraxinus excelsior* trees. *Front. Plant Sci.* **2020**, *11*, 592260. [CrossRef]
29. Line, J. The parasitism of *Nectria cinnabarina* (coral spot), with special reference to its action on red currant. *Trans. Br. Mycol. Soc.* **1922**, *8*, 22–28. [CrossRef]
30. Ghasemkhani, M.; Holefors, A.; Marttila, S.; Dalman, K.; Lehrkinder, A.; Rur, M.; Rees-George, J.; Nybom, H.; Everett, K.; Scheper, R.W.A.; et al. Real-time PCR for detection and quantification, and histological characterization of *Neonectria ditissima* in apple trees. *Trees* **2016**, *30*, 1111–1125. [CrossRef]
31. Xiwang, K.; Huang, L.; Han, Q.; Gao, X.; Kang, Z. Histological and cytological investigations of the infection and colonization of apple bark by *Valsa mali* var. *mali*. *Australas. Plant Pathol.* **2012**, *42*, 85–93.
32. Blanchette, R.A.; Biggs, A.R. *Defense Mechanisms of Woody Plants Against Fungi*; Springer: Berlin/Heidelberg, Germany, 1992; 458p.
33. Crowdy, S.H. Observations on apple canker III. The anatomy of the stem canker. *Ann. Appl. Biol.* **1949**, *36*, 483–495. [CrossRef]
34. Biggs, A.; Davis, D.; Merrill, W. Histology of cankers on *Populus* caused by *Cytospora chrysosperma*. *Can. J. Bot.* **1983**, *61*, 563–574. [CrossRef]
35. Sakamoto, Y.; Yamada, Y.; Sano, Y.; Tamai, Y.; Funada, R. Pathological anatomy of Nectria canker on *Fraxinus mandshurica* var. *japonica*. *IAWA J.* **2004**, *25*, 165–174. [CrossRef]
36. Zalasky, H. Penetration and initial establishment of *Nectria galligena* in aspen and peachleaf willow. *Can. J. Bot.* **1968**, *46*, 57–60. [CrossRef]